On the microstructure and mechanical properties of silver-bearing antibacterial CD4MCu duplex stainless steels

Xiang, Hongliang; Liu, Dong; Chen, Xueping; Cao, Huatang; Dong, XuanPu

Published in:
Materials express

DOI:
10.1166/mex.2019.1600

Publication date:
2019

Materials Express

2158-5849/2019/9/1067/009
doi:10.1166/mex.2019.1600
www.aspbs.com/mex

On the microstructure and mechanical properties of silver-bearing antibacterial CD4MCu duplex stainless steels: Solid solution temperature

Hongliang Xiang[1,2,*], Dong Liu[1], Xueping Chen[1], Huatang Cao[3], and XuanPu Dong[4]

[1] *School of Mechanical Engineering and Automation, Fuzhou University, Fuzhou 350108, P. R. China*
[2] *Jinjiang Science and Education Park of Fuzhou University, Jinjiang 362200, P. R. China*
[3] *Department of Advanced Production Engineering, Engineering and Technology Institute Groningen, University of Groningen, Nijenborgh 4, 9747AG, The Netherlands*
[4] *State Key Laboratory of Materials Processing and Die & Mould Technology, Huazhong University of Science and Technology, Wuhan 430074, China*

ABSTRACT

The Ag-bearing antibacterial stainless steel has attracted substantial attention in the field of bacterial proliferation prevention. In this study, a Cu–Ag alloy was incorporated into a CD4MCu duplex stainless steel (DSS) to produce a good antibacterial property. The Ag-bearing CD4MCu duplex stainless steel samples were conducted solid solution treatment at various temperatures. The effects of the solid solution temperature on the microstructure, mechanical and corrosion properties, as well as silver ion release characteristics and antibacterial properties were investigated. Results show that apart from the original α, γ phases, Ag-bearing phases were formed in all samples after solid solution at different temperatures. The volume fraction of γ and Ag-bearing phases decrease with increasing solution temperature. The tensile strength, hardness, elongation, and corrosion resistance first decrease and then increase along with the increase in the solid solution temperature. The heat treatment conducted at 1150 °C increases the strength, the hardness, the pitting corrosion resistance, and the antimicrobial capability simultaneously. The antibacterial rates of all the Ag-bearing CD4MCu duplex stainless steel samples after solid solution treatment are above 99%, indicating their good anti-bacterial capabilities.

Keywords: Duplex Stainless Steel, Solid Solution Temperature, Ag-Bearing Phase, Corrosion Resistance, Antibacterial Rate.

1. INTRODUCTION

Bacterial contaminations have attracted wide attention in various fields, such as food process engineering, biomedical engineering, and water-distribution systems. Thus the environment-friendly antibacterial materials have become favorable candidates for applications in these fields [1, 2].

The antibacterial metals or alloys are intriguing antibacterial materials due to their excellent comprehensive properties. Currently, in terms of stainless steel, the most common antibacterial candidate was proven to be the Cu-bearing one [3–6]. This because Cu-bearing stainless steels hold effective antibacterial effects particularly provided that certain Cu-rich phases (ε-Cu) precipitate during the antibacterial aging processing. The downside is that such Cu-rich precipitates degrade the corrosion properties of

*Author to whom correspondence should be addressed.
Email: hlxiang@fzu.edu.cn

Article

stainless steel. Alternatively, the antibacterial effect of Ag tends superior to that of Cu because even a low content of Ag in the Ag-bearing antibacterial stainless steel is potent to provide excellent antibacterial performance, and no additional antibacterial aging treatment is usually required. This is because the adsorption of Ag ions (precipitated by Ag phase) at the top of Ag-containing stainless steel to the cytoderm of the bacteria results in the distortion and rupture of the bacteria. Some Ag ions permeate the cells and intervene in the metabolism of the bacteria. Consequently, the intracellular substances flow out from the damaged cytoderm, leading to the death of the targeted bacteria eventually, suggesting the superior antibacterial property of Ag-bearing DSS.

However, current studies on the existing Ag-bearing antibacterial stainless steels are mainly limited in the ferritic stainless, austenitic stainless and martensitic stainless steels [7–10], whereas scant information has been reported on the Ag-bearing antibacterial DSS, which consists of a composite microstructure of austenite (γ) and ferrite (α) phases. DSS inherits outstanding toughness and weldability from its austenite parts and also combines the mechanical robustness, chloride resistance, and high corrosion resistance from its ferrite counterparts. The yield strength of DSS is approximately twice that of austenitic stainless steel, and it shows preponderant resistance to pitting corrosion [11–13]. Martensitic stainless steel exhibits high strength, high hardness, and low wear rate, but the poor corrosion properties due to its high carbon content extremely limits its wide use in some highly corrosive environments [14, 15]. Instead, DSS, if enhanced by suitable treatment and surface modification, could reserve high strength and hardness at no sacrifice of corrosion resistance. Thus, DSS favorably provides some combined advantages of both ferritic and austenitic stainless steels, justifying the necessity of research on it as a new Ag-bearing antibacterial candidate material. Solution treatment temperature would affect not only the phase proportion of ferrite and austenite in DSS, but also the content of alloy elements in ferrite and austenite [16]. In terms of antimicrobial activity, the higher solid solution Ag in the matrix, the better the antimicrobial property. In this study, the mechanical property, corrosion resistance, silver ion release characteristics and antibacterial property of the Ag-bearing antibacterial CD4MCu DSS were investigated. In particular, the focus point is to unveil the influence of solid solution temperature on the microstructure evolution and mechanical properties of the Ag-bearing antibacterial CD4MCu DSS. Also, we aim to provide some positive guidance for the future development of the DSS materials.

2. EXPERIMENTAL DETAILS

2.1. Materials Preparation

The Ag-bearing antibacterial CD4MCu duplex stainless steel (referred to as 1A-Ag) was prepared by melting a mixture of 316 stainless steel, ferromolybdenum, ingot iron, pure Cr and Cu, and Cu–Ag alloy in a medium frequency induction furnace. The chemical composition of the as-cast produced DSS ingot is presented in Table I.

Table I. The chemical composition of as-received steel (wt.%).

Code	C	Si	Mn	S	P	Cr	Ni	Mo	Cu	Ag	Fe
1A-Ag	0.02	0.49	0.70	0.017	0.02	26.31	5.23	2.19	3.17	0.07	Bal.

The ingots were solid solution treated in a KSS-1700 box resistance furnace at the temperature of 1050 °C, 1100 °C and 1150 °C for 2 h, respectively. The samples are coded accordingly as indicated in Table II.

2.2. Microstructural Characterization

Samples were cut in a cubic shape of 10 mm^3 from the heat-treated ingots, followed by etching in Vilella solution for 20 s prior to analysis. An Olympus-300 optical microscope (OM) and a JXA-8230 electron probe micro-analyzer (EPMA) enabled with an energy dispersive X-ray (EDX) system were utilized for the microstructural investigations.

2.3. Mechanical Property Tests

The mechanical property of the 1A-Ag steel samples after solid solution at different temperatures was studied by both tensile and hardness tests. The standard tensile samples were prepared according to the standard of GB/T228.1-2010. The tensile tests were conducted at a CMT5105 tensile apparatus with a strain rate of 2 mm s^{-1} at room temperature. For all the samples, three tests were conducted. The fracture surface of the samples was examined by a field-emission scanning electron microscopy (Nova NanoSEM, FE-SEM). The hardness tests were performed on a Rockwell hardness tester with a load of 1471 N according to the ASTM E18-2015 standard. Ten independent tests were averaged for the mean value of the hardness for each sample.

2.4. Electrochemical Tests

The 1A-Ag steel corrosion properties were investigated by the electrochemical polarization as well as the electrochemical impedance spectroscopy (EIS) tests. The tests were performed on a CHI650C electrochemical workstation with a standard three-electrode cell setup. A platinum (Pt) plate and a saturated calomel electrode (SCE) were

Table II. Solution treatment at different temperatures.

Code	Solution treatment process
1A-Ag-1050	1050 °C × 2 h + water-cooling
1A-Ag-1100	1100 °C × 2 h + water-cooling
1A-Ag-1150	1150 °C × 2 h + water-cooling

utilized as the counter electrode and the reference electrode, respectively. The working electrode was submerged in the solution with an area of 10 mm × 10 mm. The electrolyte solution was 3.5 wt.% NaCl + 96.5 wt.% distilled water. The experiments were performed in a water bath at a temperature of 30 ± 1°C. The potential range of the polarization curves ranges from −1.2 V to 1.8 V at a scanning rate of 5 mVs^{-1}. The EIS curves were obtained from a sine wave with an excitation voltage of 5 mV and a scanning frequency from 100 kHz to 10 MHz. Three independent tests of both the polarization and EIS were conducted for each sample.

2.5. Silver Ion Release Evaluation

The silver ion release characteristics of the 1A-Ag samples with solid solution treatment were measured by an Inductively Coupled Plasma–Mass Spectrometry (ICP-MS) method. The samples after different solution treatments were cut with a size of 2 mm × 20 mm × 20 mm for the tests. Then, the specimens were soaked in 0.85 wt.% NaCl solution. Periods of 3 h and 24 h were respectively selected to investigate the relationship between the soaking time and the silver ion release concentration. 10 mL maceration extract was taken and filtered with a 0.22 μm filter membrane. Then, the silver ion release concentration of maceration extract was measured by an X Series ICP-MS machine. Each measurement was conducted three times for a mean value.

2.6. Antibacterial Susceptibility Evaluation

The antibacterial properties of the 1A-Ag samples with solid solution treatment were estimated by a standard method according to the Japanese JIS Z 2801:2000 film stick method described below. As a reference, the conventional 316L stainless steel was also tested. The solution treated samples were cut with a size of 2 mm × 20 mm × 20 mm for the measurements. Note that prior to microstructural examinations, both the experimental tools and the samples were sterilized at a temperature of 121 °C for 20 min in an autoclave. The Gram-negative Escherichia coli strains were chosen as candidate bacteria for testing. The bacteria were cultured in a beef extract peptone agar overnight and consequently diluted in a beef extract peptone broth to an optical density $OD_{600\ nm}$ of 1.0 (or $2.5\sim5.0 \times 10^8$ cells mL^{-1}). The Petri dishes fitted with the sterile samples were placed on the cleansed bench. Each sample was pipetted by 100 μL of the diluted bacterial suspension. After that, the samples were covered with a sterile glass coverslip so as to obtain the same suspension contact area on the surface of each sample.

Note that all Petri dishes were incubated in a humidity incubator at a temperature of 37 ± 1 °C, and the relative humidity (R_H%) was kept constantly above 90%. Periods of 3 h and 24 h were respectively selected to investigate the relationship between the percentage of cells killed and the contact duration (namely, the reduction rate). Following the designed duration, the samples were relocated into 20 mL of a sterile eluent (the ratio of beef extract peptone broth to the normal saline is 1:500) in a sterile container, which were stirred for mixing 10 s to remove the coverslip and to attach the remaining bacteria in the eluent as well. The bacterial suspension was performed in a series of dilutions. 100 μL of aliquots of each dilution was pipetted onto the beef extract peptone agar plates, and then the bacteria were incubated overnight at a temperature of 37 ± 1 °C. The number of colonies formed units (CFU) arising from the growth of the viable bacteria at 37 ± 1 °C for 24 h showed the initial viability of bacteria that are survived in the suspension. The reduction percentage was calculated according to the Eq. (1):

$$\text{Reduction\% (CFU mL}^{-1}) = [(N_0 - N_t)/N_0] \times 100\% \quad (1)$$

where N_t is the mean CFU mL^{-1} for a tested specimen following a designated contact duration. N_0 is the mean CFU mL^{-1} for the same raw material sample at 0 h. Three tests were conducted. Three plates were spread upon from the eluent resulting from each sample.

A Phenom G2 Pro scanning electron microscope (SEM) was used to examine the structural changes of bacterial cells after different treatments at 37 ± 1 °C. All the samples for SEM observations were prepared according to the standard procedures for the biological sample fixation, namely, the samples covered with bacteria were fixed in a 2 vol.% glutaraldehyde solution at a temperature of 5 °C for 8 h and then were cleaned three times by using sterile distilled water, and each time lasted for 5 min. For the glutaraldehyde elimination, the dehydration process was performed in 30%, 50%, 70%, 80%, 95% vol.% of ethanol solutions for 10 min, respectively. Consequently, the samples were cleaned in pure anhydrous ethanol three times (30 min for each), followed by vacuum drying. Finally, the samples were pre-coated with a metallic film to avoid potential charging in SEM observations.

3. RESULTS AND DISCUSSION

3.1. Microstructural Analysis

The optical images of 1A-Ag after heat treatment are presented in Figure 1. As can be seen, apart from the original ferrite (α) and austenite (γ) phases, certain dispersed dark particles can be observed in all three samples (indicated by the arrows). In line with the phase diagram of Fe–Ag, the Ag demonstrates an extremely low solubility into steel. Therefore, the black particles are considered as Ag-rich phases or Ag-bearing phases.

Figure 1 indicates that the average diameter of the γ phase increases gradually as the solution temperature increases from 1050 to 1150 °C. This is because that the alloying elements dissolved into α and γ phases exhibit a varied distribution ratio. The distribution gradually

Article

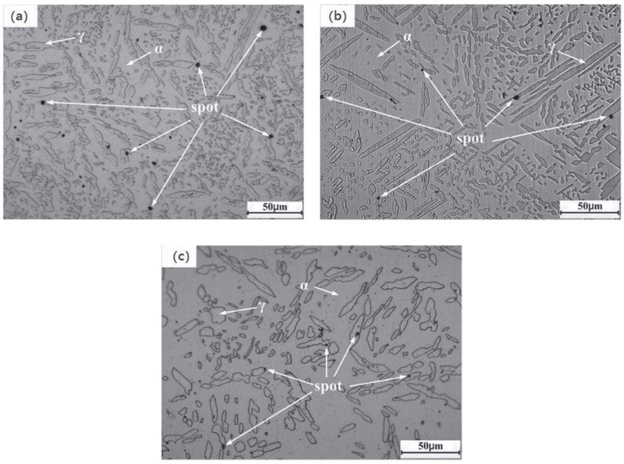

Fig. 1. Optical micrographs of (a) 1A-Ag-1050; (b) 1A-Ag-1100 and (c) 1A-Ag-1150.

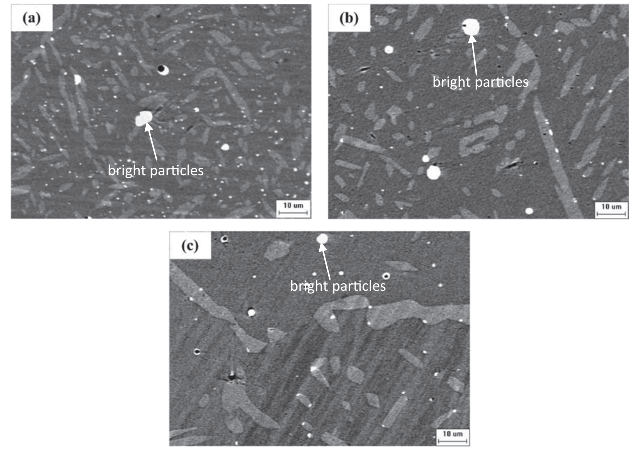

Fig. 2. SEM images of (a) 1A-Ag-1050; (b) 1A-Ag-1100 and (c) 1A-Ag-1150.

becomes uniform as the solution temperature increases. This makes α phases unstable and thereby the γ phase could transform into α phase. The volume fraction of the γ phase for three samples is presented in Table III, which was obtained according to the ASTM E562-2011 standard. Clearly, the increase in the solid solution decreases the volume fraction of the γ phase.

Figure 2 shows the 1A-Ag material consists of three different phases: α phase, γ phase, and some bright spheroidal particles. The EDS chemical composition of such particles (indicated by the arrows in Fig. 2) was listed in Table IV.

Table IV indicates that the bright particles mainly consist of Cu and Ag, together with a small amount of Fe, Cr, and Mn. It can be concluded that such bright spherical particles are in fact Ag-bearing phases, which is in accordance with the previous results [17–19]. Furthermore, the number of Ag-rich particles decreases gradually as the solution temperature increases.

Also, Figure 2 indicates that both the size and number of Ag-bearing particles change when the solid solution temperature goes up. The size of the Ag-bearing phases can be classified into two categories: granulous particles with a mean diameter below 0.5 μm and larger particles with a size ranging from 1 μm to 6 μm. The average diameters of these particles are 3.4 μm, 3.1 μm and 2.5 μm for 1A-Ag-1050, 1A-Ag-1100 and 1A-Ag-1150, respectively. The estimated volume percentage of the Ag-bearing phases is shown in Table V, showing that the volume percentage of the Ag-bearing phase decreases gradually as the solid solution temperature increases. Swartzendruber et al. [20] reported that the solid solubility of silver in steel was 0.007 wt.% at 1100 °C, whereas it increased up to 0.011 wt.% at 1150 °C. Therefore, a higher solid solution temperature is supposed to result in a higher dissolution of Ag-bearing phases.

In Figure 2 the density of Ag-bearing phases within the γ phase is lower than those within the α phase matrix and along the α/γ phase boundaries. The reason is that the crystal structures of the Cu, Ag and γ phase are all face-centered cubic (FCC), while the α phase has a body-centered cubic structure (BCC). Therefore, Cu and Ag are more compatible with the γ phase in comparison with the α phase. In conclusion, the Ag-bearing phases in Figure 2 are supposed as the inclusions formed during the solidification process.

3.2. Mechanical Properties

The tensile strength, Rockwell hardness, and elongation of the specimens are presented in Figure 3. As can be seen, at the solid solution temperature of 1050 °C, the tensile strength, the Rockwell hardness and the elongation are 725.5 MPa, 25.8 HRC and 22%, respectively, when the temperature increases to 1100 °C, they all decrease at some degrees. Furthermore, they again increase when the temperature increases up to 1150 °C, with the tensile strength and Rockwell hardness even higher than these at 1050 °C. To unravel the relationship between the microstructure and

Table III. Volume fraction ratio of γ phases in three samples (vol. %).

Code	γ phase
1A-Ag-1050	27.95
1A-Ag -1100	26.83
1A-Ag-1150	24.20

Table IV. Chemical composition of bright particles in various samples (wt. %).

Samples	Cr	Ni	Mn	Cu	Ag	Fe
1A-Ag-1050	1.72	0.81	2.53	81.04	9.56	4.33
1A-Ag-1100	2.07	1.32	2.33	82.45	7.13	4.70
1A-Ag-1150	2.10	1.45	2.21	83.45	6.06	4.72

Table V. Volume fraction of Ag-bearing phases (vol.%).

Code	Ag-bearing phase
1A-Ag-1050	1.167
1A-Ag-1100	0.875
1A-Ag-1150	0.527

mechanical properties, Figure 4 displays the fracture morphologies of the samples after tensile tests. As can been seen, a large number of dimples are clearly visible on all the tensile samples, which points to a ductile fracture model during the tensile testing.

The shallow dimples with low depth and width indicate low plasticity and vice versa. Figure 4 shows that the diameter and depth of dimples in the 1A-Ag-1050 sample is the largest, followed by the 1A-Ag-1150 sample. This suggests that the plasticity of the 1A-Ag-1050 sample is the highest, followed by the 1A-Ag-1150. Correspondingly, the 1A-Ag-1100 sample has the lowest plasticity. These results are consistent with the mechanical responses in Figure 3.

The influence of the solid solution temperature on the mechanical properties can be associated with three factors [21]: the grain size of phases, the phase ratio γ/α, and the dissolution and distribution of Ag. As the temperature increases, the number of γ phase increases moderately (see Fig. 1), which decreases the number of grain boundaries per unit volume and then the resistance to the dislocation sliding can be decreased. Consequently, the strength and plasticity of the samples reduce. Simultaneously, a further increase in solid solution temperature can promote the phase transformation of $\gamma \rightarrow \alpha$. Thus, the volume percentage of the α phase increases as the solid solution temperature increases, and this would enhance the strength of materials at the sacrifice of certain plasticity [22]. Moreover, 1A-Ag samples contain Ag-bearing phases in addition to α and γ phases. Note that the dissolution of Ag in steel increases upon the increase in the solid solution temperature, inducing some lattice distortion in the samples which potentially impedes the dislocation motion. This contributes to the solid solution strengthening effects, as

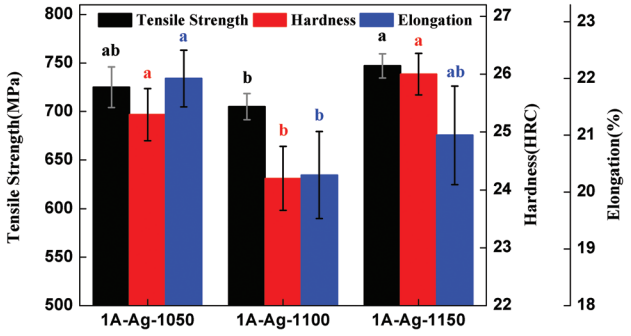

Fig. 3. Mechanical properties of three samples.

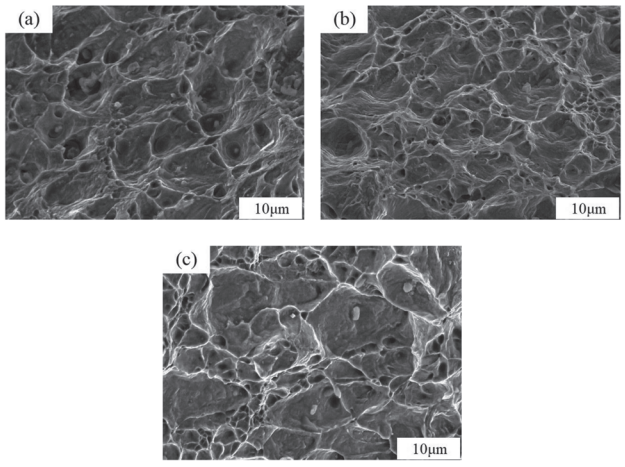

Fig. 4. Fracture morphologies of (a) 1A-Ag-1050; (b) 1A-Ag-1100 and (c) 1A-Ag-1150.

reported in our earlier work [23]. Besides, as the temperature increases, both the size and volume percentage of the Ag-bearing phases reduce, whereas the distribution of Ag in the matrix becomes more uniform. This induces the softening effects of Ag and enhances the plastic elongation [18, 19].

When the temperature increases from 1050 °C to 1100 °C, the size of the γ phase increases significantly (see Figs. 1(a) and (b)), the grain size of the γ phases plays a leading role, reducing the tensile strength, hardness as well as the plasticity of the 1A-Ag samples. When the temperature further increases from 1100 °C to 1150 °C, the volume percentage of γ and Ag-bearing phases decreases 2.63% and 0.348%, respectively, both higher than those of 1050 °C and 1100 °C (see Tables III and V). Therefore, the dual-phase ratio (γ/α), and the dissolution and distribution of Ag play a key role in influencing the tensile strength, hardness, and plasticity of the investigated 1A-Ag samples.

3.3. Corrosion Properties

3.3.1. Pitting Corrosion Resistance

The polarization curves of the investigated samples in 3.5 wt.% NaCl solution are presented in Figure 5. It can be observed that the polarization curves of all samples exhibit similar tendencies within a passive region (see the a-b part in Fig. 5). The ranges of the passive region are relatively wide, suggesting that investigated three samples all possess good passivation ability in the NaCl solution.

In line with Faraday's law [21], the corrosion rate of metals is in proportion to the corrosion current density I_{corr}, therefore the pitting corrosion resistance can be estimated by the I_{corr} value. The I_{corr} values according to the polarization curves in Figure 5 are listed in Table VI. The value of I_{corr} increases as solid solution temperature increases from 1050 °C to 1100 °C, whereas it decreases when the temperature rises to 1150 °C.

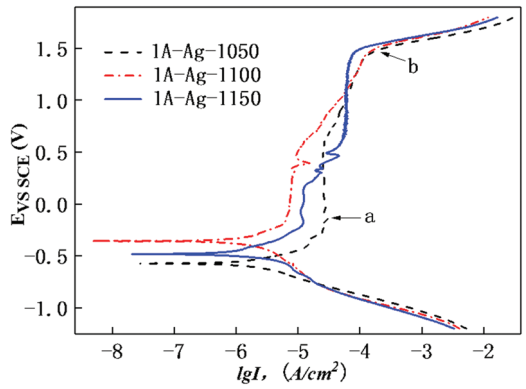

Fig. 5. Polarization curves of three samples in 3.5 wt.% NaCl solution.

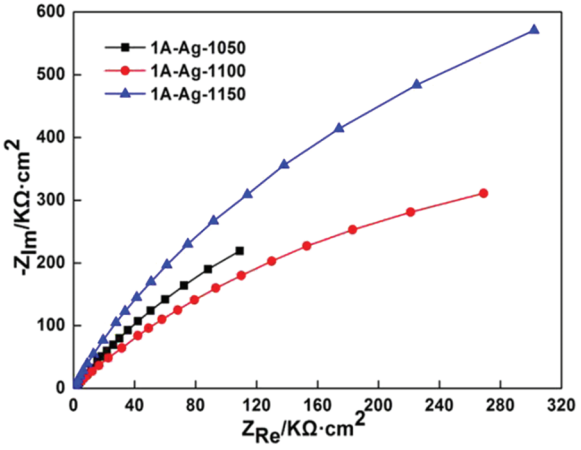

Fig. 6. Nyquist plots of three samples in 3.5 wt.% NaCl solution.

The characterization analysis (see Section 3.2) shows that the volume percentage of the α phase increases with the rising solid solution temperature. The corrosion potential of the α phase is lower than that of the γ phase in NaCl solution [22], therefore the pitting corrosion resistance of the investigated samples reduces if the volume percentage of the α phase increases. Meanwhile, the Ag-bearing phase serves as an external phase onto the passive film of the samples. This isolates the passive film on the specimen surface. The increase in the solid solution temperature also facilitates the dissolution of the Ag-bearing phases and thus reduces the volume percentage of the Ag-bearing phases. Finally, this reduces the damage of the passive film to some degree, thereby improving the pitting corrosion resistance of the samples.

It should be pointed out that as the temperature increases from 1050 °C to 1100 °C, the increase of volume fraction of the α phase starts to play an active role, and it, in fact, decreases the pitting corrosion resistance. When the temperature increases from 1100 °C to 1150 °C, the dissolution of the Ag dominates, thereby increasing the pitting corrosion resistance again. In all three samples, the value of the I_{corr} of the 1A-Ag-1150 is the lowest, confirming that the 1A-Ag-1150 sample exhibits the best pitting corrosion resistance. Our previous work [24] reported that after the same treatment, the CD4MCu DSS without Ag exhibited an I_{corr} of 1.468 $\mu A \cdot cm^{-2}$, which is lower than the I_{corr} of all the three Ag-bearing samples obtained in this study. This indicates that the pitting corrosion resistance of the Ag-bearing DSS is deteriorated by the addition of Ag, inconsistent with previous studies.

Table VI. Corrosion current density of three samples in 3.5 wt.% NaCl solution.

Code	I_{corr} ($\mu A \cdot cm^{-2}$)
1A-Ag-1050	1.881
1A-Ag -1100	2.053
1A-Ag-1150	1.675

3.3.2. Passive Film Stability

The EIS curves of the investigated samples in the 3.5 wt.% NaCl solution are presented in Figure 6. It can be seen that there is only one single capacitive reactance arc on the EIS of all samples, indicating that a relatively complete passivation film can be formed on the surface of all specimens. The EIS curves in Figure 6 were fitted by the ZSimpWin software to obtain the relevant characterization parameters of the electrochemical process. The R_s (QR_t) model was utilized as the equivalent circuit due to the best fitting, the Figure 7 is the schematic diagram of equivalent circuit drawn by us according to ZSimpWin software fitting. R_s is the solution resistance, and R_t is the charge transfer resistance associated with the stability of the passive film, respectively. The higher the value of the R_t, the more difficult the charge migration at the interfaces between the electrode and the electrolyte solution. As a consequence, less damage would be inflicted on the passive film. The impedance Z_Q can be determined by Eq. (2):

$$Z_Q = (jw)^{-n}/Y_0 \quad (2)$$

where Q is the constant phase angle element; $j = \sqrt{-1}$; ω is the angular frequency; n is the apparent diffusion coefficient, which represents the degree of the dispersion effects at the surface of the working electrode; Y_0 is the admittance, which represents the corrosion current density generated from the surface of the working electrode. The

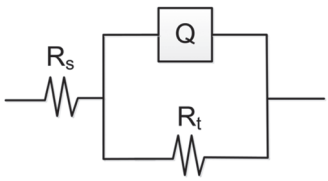

Fig. 7. Equivalent circuit of samples in 3.5 wt.% NaCl solution.

Table VII. Values of EIS fitting parameters in R(QR) equivalent circuits.

Code	R_s ($\Omega \cdot cm^2$)	Y_0 ($S \cdot sec^{\wedge} n/cm^2$)	n	R_t ($\Omega \cdot cm^2$)
1A-Ag-1050	3.815	5.918×10^{-5}	0.7385	1.473×10^5
1A-Ag -1100	3.320	9.135×10^{-5}	0.7687	9.296×10^4
1A-Ag-1150	3.835	5.141×10^{-5}	0.8000	1.864×10^5

lower the value of Y_0, the higher the resistance of the electrode surface and the lower the corrosion current density will be.

The fitting results are presented in Table VII. No significant changes in the R_s and n can be observed. This indicates that all the tested systems are relatively stable. Then the temperature increases, the value of Y_0 increases first and then decreases. However, the value of R_t shows a totally opposite trend; i.e., it decreases first and then increases. An increase in the corrosion current density followed by a decline is observed, and the stability of the passive film presents the opposite trend. All these suggest that the corrosion resistance of the investigated samples decreases first and increases later as the solid solution temperature increases to 1150 °C. Meanwhile, the value of the Y_0 for the 1A-Ag-1150 is the lowest, while that of the R_t is the highest in all samples, indicating that the 1A-Ag-1150 sample has the highest corrosion resistance. This is consistent with the results of the polarization curves (Fig. 5).

3.4. Antibacterial Properties

Table VIII shows the Ag ion release concentration of the 1A-Ag samples after soaking in 0.85 wt.% NaCl solution for a different time. As shown in Table VIII, the Ag ion release concentration of the three Ag-bearing samples after 3 h and 24 h in 0.85 wt.% NaCl solution are compared in Table VIII, indicating an increasing tendency of the Ag ion release concentration as the solid solution temperature increases. The Ag ion release concentration of the 1A-Ag samples after 24 h is higher than that of the 1A-Ag samples after 3 h, indicating an increasing tendency of the Ag ion release concentration as the soaking time increases.

Figure 8 presents the effects of bacteria inhibition of the samples and 316L stainless steel in contact with the Gram-negative Escherichia coli for 3 h. Figure 8(a) confirms a large number of viable bacteria have formed a lawn on the agar. This is because the 316L stainless steel itself does not have any antibacterial properties [23]. However, in Figures 8(b–d), all the three Ag-bearing samples exhibit outstanding antibacterial behavior, as confirmed by that after 3 h almost no bacteria are found survived.

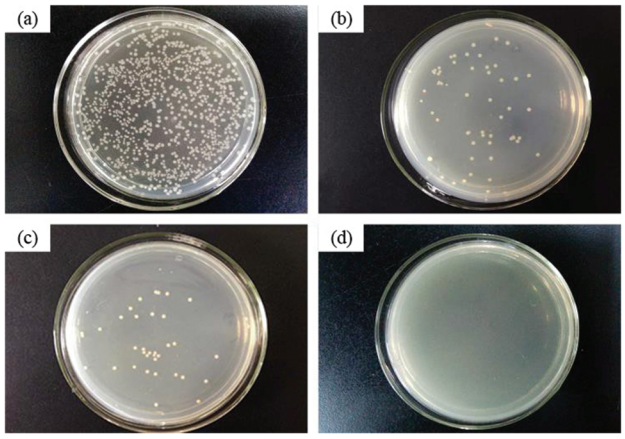

Fig. 8. Colony forming units (CFU) of viable bacteria after 3 h contact with the surfaces of (a) 316L, (b) 1A-Ag-1050; (c) 1A-Ag-1100 and (d) 1A-Ag-1150.

Table IX presents the number of viable bacteria and the corresponding antibacterial rate of the samples after contacting with the bacteria for 3 h and 24 h, respectively. It is found that the number of the viable bacteria on all three Ag-bearing sample surfaces is lower than that of 10 CFUs even after 24 h, and the antibacterial rate exceeds 99.9%. In line with the Japanese JIS Z 2801:2000 standard, this points to a strong antibacterial effect. Our previous work [25] reported that after the same treatment, the CD4MCu duplex stainless steel exhibited an antibacterial rate of 16.7%, far lower than 99.9% obtained in this study. Therefore, the Ag-bearing phases dispersedly distributed over the Ag-bearing antibacterial CD4MCu duplex stainless steel are supposed to play a profound role in the bacterial inhibition. Meanwhile, the different antibacterial rates of the three Ag-bearing samples after 3 h in the bacterial liquid are compared in Table IX. The values are 99.4%, 99.6%, and 99.9%, respectively, indicating an increasing tendency of the antibacterial rate as the solid solution temperature and Ag ion release concentration increase. It is well-known that the antibacterial property of the Ag-bearing samples is due to the dissolution of

Table VIII. Ag ion release concentration of samples under different time in 0.85 wt.% NaCl solution.

	Ag ion release concentration/(ppb)	
Code	3 h	24 h
1A-Ag-1050	0.043	0.141
1A-Ag-1100	0.062	0.219
1A-Ag-1150	0.099	0.398

Table IX. Antibacterial rates (R) of four samples under different time in bacteria liquid.

	Bacteria count/($cfu \cdot mL^{-1}$)		R/(%)	
Code	3 h	24 h	3 h	24 h
316L	9.50×10^5	9.50×10^5	–	–
1A-Ag-1050	5.5×10^3	<10	99.4	99.9
1A-Ag-1100	3.5×10^3	<10	99.6	99.9
1A-Ag-1150	<10	<10	99.9	99.9

Article

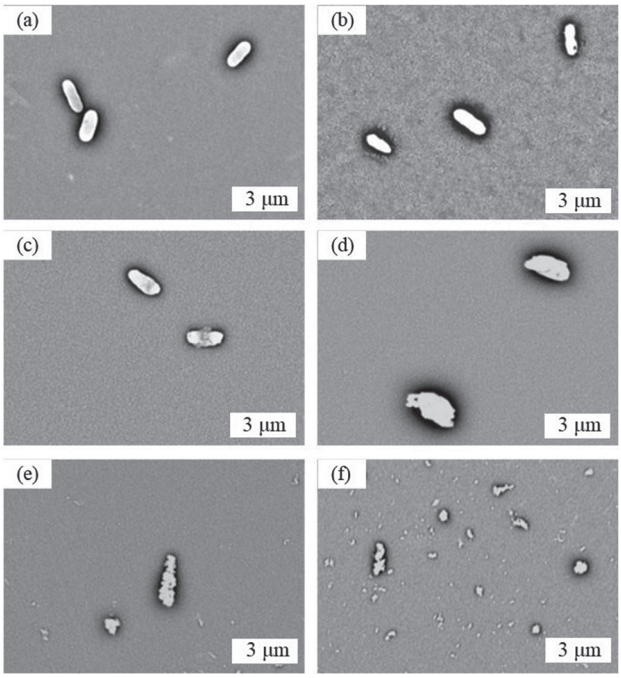

Fig. 9. Morphology evolution of Escherichia coli on 316L for (a) 0 h; (b) 24 h; and on the 1A-Ag-1150 for (c) 1 h; (d) 3 h; (e) 5 h and (f) 24 h treatment.

Ag ions penetrating into the bacterial cells. As analyzed above, the distribution of Ag in the matrix become rather uniform as the solution temperature increases. The Ag ions react with the bacteria that are adsorbed on the surface of the steel, thereby retarding the bacteria metabolism and consequently inhibiting the growth and reproduction of bacteria [7, 26–29].

Figure 9 shows the morphologies of the Escherichia coli cells at the top surface of the investigated samples and the conventional 316L stainless steel after different exposure time. It is clear that the cell shapes on the surface of the 316L treated for 0 h and 24 h are both well-defined. All these cells present rod-like or plump thallus shapes (Figs. 9(a and b)), suggesting that the cells are in normal sound conditions, free from any traceable environmental attacks, and they survive well after 24 h exposure. On the contrary, significant morphological changes occur in the Escherichia coli cells on the surface of the 1A-Ag-1150 specimens after 1 h, 3 h, 5 h, and 24 h exposure, as presented in Figures 9(c) and (d). Figure 9(c) shows the cell bacterial morphologies become irregular. In some cells, the walls and membranes are obviously damaged, which causes the cytoplasm to drain out, and this explains for the bacterial apoptosis. From Figure 9(d), we can see that the shapes of most bacterial become distinctly abnormal after 3 h, and almost all bacteria are killed, as listed in Table IX. For the samples in the bacteria liquid for 5 h and 24 h (Figs. 9(e and f)), most bacterial cells appear seriously damaged, broken and even shattered ultimately.

4. CONCLUSIONS

The microstructure of the Ag-bearing antibacterial CD4MCu DSS consists of new Ag-bearing phases in addition to original α and γ phases from the matrix. The Ag-bearing phases largely control the corrosion resistance. The content of Ag in the Ag-bearing phases and the number of the Ag-bearing phase decrease as the solid solution temperature increases. The tensile strength, hardness, and elongation of the Ag-bearing antibacterial CD4MCu DSS decrease first and increase as the solution temperature increases. It is the same for the corrosion current density of the Ag-bearing antibacterial CD4MCu DSS in the 3.5 wt.% NaCl solution. The stability of passive film, however, decreases first and then increases as the temperature increases, and the corrosion resistance also follows the trend.

The Ag ion release concentration increases as temperature and soaking time increase. The antibacterial rates of the Ag-bearing antibacterial CD4MCu duplex stainless steel are 99.4%, 99.6% and 99.9% after 3 h exposure to the bacteria liquid of the Escherichia coli in the samples with the solution temperature being 1050 °C, 1100 °C, and 1150 °C, respectively. All the rates reach 99.9% after 24 h exposure. The bacterial morphologies of the Escherichia coli become abnormal on contacting with the Ag-bearing antibacterial CD4MCu DSS, and certain cells are finally destroyed.

Acknowledgments: This work was financially supported by the National Natural Science Fund of China (No. 51601039); Major Projects Fund from Fujian (No. 2017HZ0001-2); Industrial Technology Joint Innovation Projects of Fujian (No. FG-2016001) and the Advanced Metal Materials and Forming Technology Innovation Team.

References and Notes

1. Zhang, Z.X. and Xu, Z., **2007**. Microstructures and properties of copper (nitrogen)-bearing antibacterial stainless steel. Ph.D. Thesis, Shanghai Jiao Tong University.
2. Wang, J.J., Li, Z.Y., Liang, Y.Q., Zhu, S.L., Cui, Z.D., Bao, H.J., Liu, Y.D. and Yang, X.J., **2015**. Cytotoxicity and antibacterial efficacy of silver nanoparticles deposited onto dopamine-functionalized titanium. *Materials Express*, *5*(3), pp.191–200.
3. Oguzie, E.E., Li, J.B., Liu, Y., Chen, D.M., Li, Y., Yang, K. and Wang, F.H., **2010**. Electrochemical corrosion behavior of novel Cu-containing antimicrobial austenitic and ferritic stainless steels in chloride media. *Journal of Materials Science, 45*(21), pp.5902–5909.
4. Li, M.J., Li, N., Xu, D.K., Ren, G.G. and Yang, K., **2015**. Antibacterial performance of a Cu-bearing stainless steel against microorganisms in tap water. *Journal of Materials Science & Technology, 31*(3), pp.243–251.
5. Nan, L., Xu, D.K., Gu, T.Y., Song, X. and Yang, K., **2015**. Microbiological influenced corrosion resistance characteristics of a 304L-Cu stainless steel against Escherichia coli. *Materials Science & Engineering C, 48,* pp.228–340.

Article

6. Xi, T., Yang, C.G., Shahzad, M.B. and Yang, K., **2015**. Study of the processing map and hot deformation behavior of a Cu-bearing 317LN austenitic stainless steel. *Materials & Design, 87,* pp.303–312.
7. Sreekumari, K.R., Nandakumar, K., Takao, K. and Kikuchi, Y., **2003**. Silver containing stainless steel as a new outlook to abate bacterial adhesion and microbiologically influenced corrosion. *ISIJ International, 43*(11), pp.1799–1806.
8. Liao, K.H., Ou, K.L., Cheng, H.C., Lin, C.T. and Peng, P.W., **2010**. Effect of silver on antibacterial properties of stainless steel. *Applied Surface Science, 256*(11), pp.3642–3646.
9. Yuan, J.P. and Li, W., **2013**. Antibacterial 316L stainless steel containing silver and niobium. *Rare Metal Materials and Engineering, 42*(10), pp.2004–2008.
10. Xuan, Y., Zhang, C., Fan, N.Q. and Yang, Z.G., **2014**. Antibacterial property and precipitation behavior of Ag-added 304 austenitic stainless steel. *Acta Metallurgica Sinica (English Letters), 27*(3), pp.539–545.
11. Song, Z.G., Feng, H. and Hu, S.M., **2017**. Development of Chinese duplex stainless steel in recent years. *Journal of Iron and Steel Research International, 24*(2), pp.121–130.
12. Zhao, Y., Wang, Y., Li, X., Zhang, W., Tang, S. and Liu, Z., **2018**. Effects of plastic straining on the corrosion resistance of TRIP-aided lean duplex stainless steels. *Journal of Materials Science, 53*(12), pp.9258–9272.
13. Llorca-Isern, N., Biserova-Tahchieva, A., Lopez-Jimenez, I., Calliari, I., Cabrera, J.M. and Roca, A., **2019**. Influence of severe plastic deformation in phase transformation of super duplex stainless steels. *Journal of Materials Science, 54*(3), pp.2648–2657.
14. Zong, X.M., Jiang, W.M. and Fan, Z.T., **2018**. Characteristics and wear performance of borided AISI 440C martensitic stainless steel. *Materials Express, 8*(6), pp.500–510.
15. Maria, G.G.B., Pedroso, C.A.D., Rodrigues, D.G. and Santos, D.B., **2017**. Strain-induced martensite and reverse transformation in 2304 lean duplex stainless steel and its influence on mechanical behavior. *Steel Research International, 90*(3), p.1800437.
16. Zhao, J.L., Yang, C.G., Zhang, D.W., Zhao, Y., Khan, M.S., Xu, D.K., Xi, T., Li, X.G. and Yang, K., **2016**. Investigation on mechanical, corrosion resistance and antibacterial properties of Cu-bearing 2205 duplex stainless steel by solution treatment. *RSC Advances, 6*(114), pp.112738–112747.
17. Morrison, W.B., **1985**. Influence of silver on structure and properties of low-carbon steel. *Materials Science and Technology, 1*(11), pp.954–960.
18. Chiang, W.C., Tseng, I.S., Møller, P., Hilbert, L.R. and Nielsen, T.T., **2010**. Influence of silver additions to type 316 stainless steels on bacterial inhibition, mechanical properties, and corrosion resistance. *Materials Chemistry and Physics, 119*(1), pp.123–130.
19. Huang, C.F., Chiang, H.J., Lan, W.C., Chou, H.H., Ou, K.L. and Yu, C.H., **2011**. Development of silver-containing austenite antibacterial stainless steels for biomedical applications part I: Microstructure characteristics, mechanical properties and antibacterial mechanisms. *Biofouling, 27*(5), pp.449–570.
20. Swartzendruber, L.J., **1984**. The Ag-Fe (Silver-Iron) system. *Journal of Phase Equilibria, 5(6),* pp.560-564.
21. Cao, C.N., **2008**. *Principle of Corrosion Electrochemistry*, Third edition. Beijing, Chemical Industry Press.
22. Fu, Y., Lin, C.J. and Cai, W.D., **2005**. A study of the selective dissolution behavior of duplex stainless steel by micro-electrochemical technique. *Acta Metallurgica Sinica, 41*(3), pp.302–306.
23. Yang, P.A., **2016**. Study on surface modification and its biological properties of 316L stainless steel. Master Thesis, Donghua University.
24. Guo, P.P., **2013**. Preparation, microstructures and properties of the silver-bearing antibacterial duplex stainless steel. Master Thesis, Fuzhou University.
25. Xiang, H.L., Guo, P.P. and Liu, D., **2014**. Microstructure and antibacterial properties of Ag-bearing duplex stainless steel. *Acta Metallurgica Sinica, 50*(10), pp.1210–1216.
26. Feng, Q.L., Wu, J., Chen, G.Q., Cui, F.Z., Kim, T.N. and Kim, J.O., **2000**. A mechanistic study of the antibacterial effect of silver ions on Escherichia coli and Staphylococcus aureus. *Journal of Biomedical Materials Research, 52*(4), pp.662–668.
27. Lee, D., Cohen, R.E. and Rubner, M.F., **2005**. Antibacterial properties of Ag nanoparticle loaded multilayers and formation of magnetically directed antibacterial microparticles. *The ACS Journal of Surfaces and Colloids, 21*(21), pp.9651–9659.
28. Chen, R.S., Ni, H.W., Zhang, H.S., Yue, G., Zhan, W.T. and Xiong, P.Y., **2013**. A preliminary study on antibacterial mechanisms of silver ions implanted stainless steel. *Vacuum: Technology Applications & Ion Physics: The International Journal & Abstracting Service for Vacuum Science & Technology, 89,* pp.249–253.
29. Araújo, E.A., Andrade, N.J., Da Silva, L.H.M., Bernardes, P.C., Teixeira, A.V.N.D., de Sa, J.P.N., Fialho Jr., J.F.Q. and Fernandes, P.E., **2012**. Antimicrobial effects of silver nanoparticles against bacterial cells adhered to stainless steel surfaces. *Journal of Food Protection, 75*(4), pp.701–705.

Received: 31 March 2019. Accepted: 24 September 2019.